Characterizations and source analysis of atmospheric inorganic ions at a national background site in the northeastern Qinghai-Tibet Plateau: insights into the influence of anthropogenic emissions on a high-altitude area of China

Bin Han[1], Jing Wang[1], Xueyan Zhao[1], Baohui Yin[1], Xinhua Wang[1], Xiaoyan Dou[2], Wen Yang[1], Zhipeng Bai[1]

1. State Key Laboratory of Environmental Criteria and Risk Assessment, Chinese Research Academy of Environmental Sciences, Beijing, China
2. Qinghai Environmental Monitoring Center, Xining, Qinghai, China

Abstract

Atmospheric particulate matter (PM) imposes highly uncertain impacts on both radiative forcing and human health. While ambient PM has been comprehensively characterized in China's megacities; its composition, source, and characteristics in the Qinghai-Tibet Plateau (QTP) are not yet fully understood. An autumn observational campaign was conducted during the 1st - 15th October 2013 at a national background monitoring station (3295 m a.s.l.) in the QTP. Real time concentrations of inorganic water-soluble ions (WSIs) associated with $PM_{2.5}$ were measured in addition to $PM_{2.5}$ concentrations, gaseous pollutants, and meteorological parameters. SO_4^{2-} was the most abundant WSI (10.00 ±4.39 μg/m^3) followed by NH_4^+ (2.02 ±0.93 μg/m^3), and NO_3^- (1.65 ±0.71 μg/m^3). Observed WSI concentrations were lower as compared to urban sites in eastern China; however, they were higher as compared to other QTP monitoring sites. To better understand the potential sources of WSIs in the QTP, a Positive Matrix Factorization receptor model was used. Results showed that mixed factor including animal waste emission and biomass burning, crustal dust, salt lake emissions, secondary sulfate and secondary nitrate were the major emission sources of particulate inorganic ions at the study site. Correlation analysis between WSIs revealed that NH_4NO_3, $(NH_4)_2SO_4$, Na_2SO_4, and K_2SO_4 were the major atmospheric aerosol components. High sulfate and nitrate oxidation ratios indicated strong secondary formation of both SO_4^{2-} and NO_3^-. Both photochemical and heterogeneous reactions contributed to the formation of particulate SO_4^{2-}, while the conversion of NO_2 to NO_3^- only occurred via photochemical reactions in the presence of high O_3 concentrations and strong sunlight.

1. Introduction

Atmospheric aerosol has a significant impact on climate change and human health, the extent of which is determined by their physical and chemical properties. High concentrations of aerosols are associated with rapid economic growth, urbanization, industrialization, and motorization, and have become a major environmental concern in China (Du et al., 2015). Extensive research has investigated the sources, chemical and physical properties, and evolution processes of aerosol particles at urban and rural sites in China during the last decade (Cao et al., 2007; Gong et al., 2012; He et al., 2011; Jiang et al., 2015; Sun et al., 2015; Sun et al., 2013; Wu et al., 2007). These studies indicated that fine particles are mainly composed of organics, sulfate, nitrate, ammonium, mineral dust, and black carbon. While these studies have greatly improved our understanding on the sources and physical/chemical properties of aerosol particles, they were predominantly conducted in developed areas of China, including Beijing–Tianjin–Hebei, the Pearl River Delta, and the Yangtze River Delta. In remote areas, such as the Qinghai-Tibet Plateau (QTP), studies on atmospheric aerosol properties are rare.

The QTP covers most of the Tibet Autonomous Region and Qinghai Province in western China, with an area of 5,000,000 km^2 and an average elevation over 4000 m. The area is geomorphologically the largest and highest mountain region on earth (Yao et al., 2012). Described as the "water tower" of Asia, this area contains the headwaters of the Mekong, Yangtze, and Yellow Rivers. Therefore, climate variability and change in this region has fundamental impacts on a range of climate-related ecosystem services (McGregor, 2016). Due to its unique ecosystem, landforms, and monsoon circulation, the QTP has a profound role in regional and global atmospheric circulation, radiative budgets, and climate systems (Su et al., 2013; Kopacz et al., 2011; Yang et al., 2014; Jin et al., 2005). Limited anthropogenic activity, a sparse population, immense area, and high elevation mean that, alongside the Arctic and Antarctic, the QTP is considered one of the most pristine terrestrial regions in the world. Because of this, the region is an ideal location for characterizing background aerosol properties, regional and global radiative forcing, climate and ecological changes, and the transportation of global air pollutants. Thus, a comprehensive understanding of QTP aerosol chemistry is crucial for assessing anthropogenic influences and evaluating long-term changes in the global environment (Cong et al., 2015; Zhang et al., 2012).

Research relating to the chemical and physical characteristics of aerosols in the QTP is rare; hence, their sources, properties, and evolution processes are poorly understood. This lack of research is a result of the region's remoteness and challenging weather conditions. Most previous studies of aerosol chemistry in the QTP were conducted in the Himalaya (the southeastern or southern areas of the QTP) to assess the key roles of the Himalaya on regional climate and the environment, as well as the boundary transportation of air pollutants from South Asia (Cong et al., 2015; Zhao et al., 2013b; Wan et al., 2015; Shen et al., 2015). Conversely, the northeastern QTP, located in inland China, is likely to have very different atmospheric

behaviors as compared to those of the Himalaya due to different climate patterns and aerosol sources between the two regions (Xu et al., 2015).

Two decades ago, natural emission and occasional perturbations from human activities were believed to be the major sources of particles in this area. (Wen et al., 2001; Gao and Anderson, 2001; Tang et al., 1999). With enlargement of human activities in recent years, several studies found that SO_4^{2-}, NO_3^-, NH_4^+, and Ca^{2+} were major water-soluble ions (WSIs) (Xu et al., 2014; Li et al., 2013; Zhang et al., 2014), suggesting that both anthropogenic pollution and mineral dust contributed to the total mass of $PM_{2.5}$. Recent real time observation also proved that sulfate, which is regarded as one of the marker of anthropogenic emission, was dominant in PM_1 mass in this area (Du et al., 2015). Despite some researches have been done in this area, there are still some scientific gaps on the aerosol chemical properties. Most of previous studies were based on the manual filter sampling, with the duration ranging from days to weeks (Du et al., 2015). These low temporal resolution data have limitations when being used for characterizing the rapid variations of chemical compositions and capturing secondary aerosol formations. Data from the high resolution instruments offer significant advantages over traditional filter-based measurements (Vedantham et al., 2014). To our knowledge, real-time measurements of aerosol particle composition at rural sites in the Tibetan Plateau are still rare (Du et al., 2015).

WSIs comprise a large portion of aerosol particles and may help understand chemical reactions in the atmosphere (Tripathee et al., 2017). They can provide important information for understanding chemical characterizations, sources, behaviors, and formation mechanisms; and hence, knowledge on the emission of gaseous precursors and the effect of regional and local pollution on ecosystem health (Wang et al., 2005; Tripathee et al., 2016). Furthermore, WSIs regulate the electrical properties of the atmospheric medium, participate in ion-catalyzed and ion–molecule reactions, and contribute to physicochemical interactions, including ion-induced new particle formation (Frege et al., 2017; Schulte and Arnold, 1990). Given the importance of WSIs on aerosol properties and the limited data on aerosol chemical compositions in the QTP, more WSIs data are needed to better characterize the chemical composition of aerosols in this area.

In our study, a real time monitor for WSIs associated with $PM_{2.5}$ was deployed at a national background monitoring site (Menyuan, Qinghai, 37º36'30''N, 101º15'26''E; 3295 m a.s.l.) in the northeastern QTP, following Du et al. (2015). Hourly mass concentrations of $PM_{2.5}$ bound sulfate, nitrate, ammonium, sodium, potassium, magnesium, and calcium were obtained during the 1st –15th October 2013. Real time measurements of SO_2, NO_X, CO, O_3, $PM_{2.5}$, and meteorological parameters were also recorded. We discuss the characterization and variation of WSIs; analyze the potential formation mechanisms of particulate SO_4^{2-} and NO_3^-, and investigate potential aerosol sources by combining WSI and gas pollutant data.

2. Methods

2.1 Monitoring site

Figure 1 shows the location of the monitoring site at the peak of Daban Mountain, Menyuan Hui Autonomous County, Qinghai Province (37º36'30''N, 101º15'26''E; 3295 m a.s.l.). The site is owned by the Chinese national atmospheric background monitoring station system and is approximately 160 km north of Xining, the capital city of Qinghai Province. This monitoring site is also approximately 100 km northeast of Qinghai Lake, a saline and alkaline water body that is the largest lake in China. The area is characterized by a typical plateau continental climate with an annual temperature of 0.8 ºC and precipitation of 520 mm. Meteorological parameters during the observation period are summarized in Table 1. The site is surrounded by typical QTP vegetation, including potentilla fruticosa and kobresia. No strong anthropogenic emission sources exist in the adjacent area, with the exception of occasional biomass burning events and yak dung burning for residential cooking and heating. A national road (G227) and a provincial road (S302) to through the area of this site, however, the traffic volume around the site is small (Du et al., 2015).
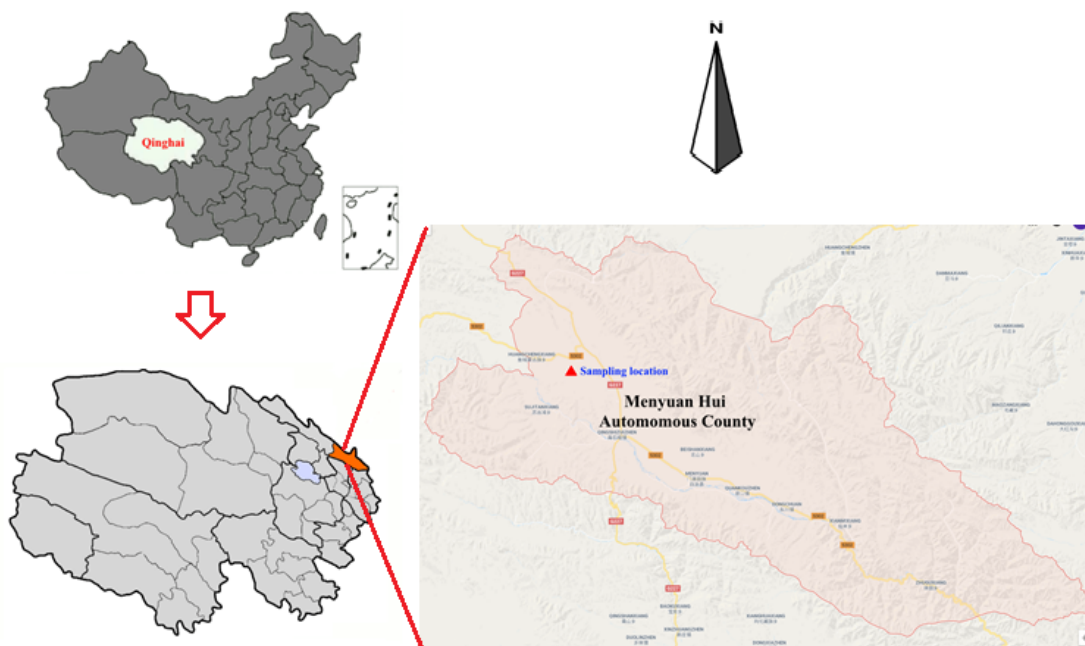
Figure 1 Location of sampling site

2.2 Instruments

Hourly concentrations of NO_3^-, SO_4^{2-}, Na^+, NH_4^+, K^+, Mg^{2+}, and Ca^{2+} associated with $PM_{2.5}$ were simultaneously measured by an ambient ion monitor (Model URG 9000B, URG Corporation, USA). A set of commercial instruments from Teledyne API (USA) were equipped to measure hourly concentrations of SO_2 (M100EU, detection limit: 50 ppt), $NO/NO_2/NO_x$ (M200EU, detection limit: 50 ppt), CO (Model 300EU, detection limit: 20 ppb), and O_3 (Model 400E, detection limit: 0.6 ppb). Hourly $PM_{2.5}$ concentrations were measured using an Ambient Dust Monitor 365

149 (GRIMM; Grimm Aerosol Technik GmbH &Co. KG, Ainring, Germany).
150 Meteorological parameters (e.g. temperature, relative humidity, pressure, and wind
151 speed and direction) were also recorded.
152
153 **2.3 data analysis**
154 2.3.1 Oxidant ratio
155 Particulate sulfate and nitrate oxidation ratios (SOR and NOR, respectively),
156 defined as the molar ratio of SO_4^{2-} and NO_3^- to total oxidized sulfur and nitrogen
157 (Zhou et al., 2009), were used to evaluate secondary conversion from NO_2 and SO_2 to
158 NO_3^- and SO_4^{2-}, respectively. High SOR and NOR indicate larger conversions of SO_2
159 and NO_x to their respective particulate forms in $PM_{2.5}$. In this study, NOR and SOR
160 were calculated based on the following formulae:

$$SOR = \frac{[SO_4^{2-}]}{[SO_2]+[SO_4^{2-}]} \quad (1)$$

161

$$NOR = \frac{[NO_3^-]}{[NO_2]+[NO_3^-]} \quad (2)$$

162

163 Given that there potentially exist the direct emissions of sulfate and nitrate (such
164 as the sulfate released from the salt lake, which will be discussed in the source
165 apportionment section), it is not suitable to apply their concentrations directly into the
166 formulae (1) and (2). Therefore, we used the PMF model to calculate the
167 concentrations of secondary sulfate and nitrate in each observation, and then take
168 these modeled concentrations to estimate the SOR and NOR. The PMF model will be
169 introduced in following section.
170 2.3.2 Ion balance
171 Ion balance was used to evaluate the acid-base balance of aerosol particles. We
172 converted the WSIs mass concentration into an equivalent concentration, as follows:

$$C \ (cation, \mu eq/m^3) = \frac{Na^+}{23} + \frac{NH_4^+}{18} + \frac{K^+}{39} + \frac{Mg^{2+}}{12} + \frac{Ca^{2+}}{20} \quad (3)$$

173

$$A \ (anion, \mu eq/m^3) = \frac{SO_4^{2-}}{48} + \frac{NO_3^-}{62} \quad (4)$$

174

175

176 2.3.3 Source apportionment
177 Positive Matrix Factorization (PMF), developed by Paatero (Paatero and Tapper,
178 1994; Paatero, 1997), has been widely applied in source apportionment researches. In
179 this model, a data matrix X_{ij}, in which i is the sample and j is the measured chemical
180 species, can be viewed as a speciated data set, and the concept of this model can be
181 represented as:

$$X_{ij} = \sum_{k=1}^{p} g_{ik}f_{kj} + e_{ij} \quad (5)$$

182

183 where p is the number of factors; f is the chemical profile of each source, g is
184 the mass contribution of each factor to the sample; f_{jk} is the source profile, and e_{ij}
185 is the residual for each species or sample.
186 PMF solves Eq (5) by minimizing the sum of the square of residuals weighted
187 inversely with the error estimates of the data points, Q, defined as:

$$Q = \sum_{i=1}^{n} \sum_{j=1}^{m} \left[\frac{x_{ij} - \sum_{k=1}^{p} g_{ik} f_{kj}}{u_{ij}} \right]^2 \quad (6)$$

where u_{ij} is the uncertainty of chemical species j in sample i.

Furthermore, we used the results of the source apportionment to estimate the concentrations of secondary sulfate and nitrate and then applied them in the calculations of SOR and NOR. By running the PMF model, we identified the secondary sulfate and nitrate in factor s and t, respectively. We also obtained the hourly contributions of each factor to the total ions, as well as the profile of each factor. Then the products of hourly contributions of factor s or t and the percentages of sulfate or nitrate in the profile of factor s or t are taken as the concentrations of secondary sulfate or nitrate. The calculation is defined as:

Presume that factor s and t are the secondary sulfate and nitrate sources calculated by the PMF model ($s, t \leq p$), then:

$$Contribution_{i,secondary\ sulfate} = g_{i,s} \times r_{s,sulfate} \quad (7)$$

$$Contribution_{i,secondary\ nitrate} = g_{i,t} \times r_{t\ nitrate} \quad (8)$$

where $g_{i,s}$ is the contribution of factor s to sample i, while $g_{i,t}$ is the contribution of factor t to sample i; and $r_{s,sulfate}$ is the ratio of $sulfate$ in the factor s, while $r_{t,nitrate}$ is the ratio of $nitrate$ in the factor t.

2.3.4 Statistical analysis

Correlation analysis, analysis of variation (ANOVA), and linear regression were applied. All statistical calculations were preformed using R studio software packages (Version 0.99.903, RStudio, Inc.).

3. Results and Discussion

3.1 Descriptive analysis

Table 1 summarizes the concentrations of WSIs, $PM_{2.5}$, and gaseous pollutants and data of meteorological parameters during the observation period. SO_4^{2-} accounted for 67.9% of the total WSIs mass, followed by NH_4^+ (13.7%), and NO_3^- (11.2%). SO_4^{2-}, NO_3^- and NH_4^+ (SNA), accounting for 92.8% of the total WSIs mass, were the major components of secondary inorganic aerosols.

217   Table 1 Descriptive statistics of WSIs species, gaseous pollutants and meteorological parameters

Species	Mean	Standard Deviation	Percentile				
			5th	25th	50th	75th	95th
WSIs (μg/m³)							
NO_3^-	1.65	0.71	0.62	1.14	1.60	2.02	2.90
SO_4^{2-}	10.00	4.39	6.39	7.05	8.37	10.73	18.83
Na^+	0.86	0.61	0.01	0.50	0.79	1.12	1.66
NH_4^+	2.02	0.93	0.52	1.40	1.95	2.54	3.59
K^+	0.05	0.03	0.01	0.03	0.04	0.06	0.11
Mg^{2+}	0.06	0.19	0.01	0.02	0.04	0.05	0.09
Ca^{2+}	0.09	0.05	0.01	0.05	0.09	0.11	0.18
Air pollutants (μg/m³)							
$PM_{2.5}$	18.99	13.10	2.60	9.00	16.15	26.35	44.28
SO_2	4.37	5.76	1.28	1.79	2.40	3.88	14.70
NO	0.12	0.19	0.01	0.02	0.04	0.13	0.45
NO_2	4.35	2.66	1.42	2.58	3.96	5.26	8.99
NO_X	4.45	2.70	1.42	2.68	4.14	5.33	9.02
CO	48.59	56.51	4.60	13.65	26.31	58.35	183.57
O_3	107.71	25.13	82.91	92.74	106.93	117.72	134.02
Acidity (μeq/m³)							
Anion	0.22	0.11	0.01	0.17	0.19	0.26	0.42
Cation	0.13	0.08	0.00	0.05	0.14	0.17	0.25
Oxidation Ratio							
SOR	0.55	0.18	0.23	0.43	0.56	0.65	0.88
NOR	0.16	0.08	0.07	0.11	0.15	0.20	0.30
Meteorological Parameters							
Temp (°C)	6.55	4.53	0.50	2.80	5.60	10.70	14.49
RH (%)	52.92	18.44	22.56	38.40	55.80	65.80	81.56
Pressure (kPa)	68.58	0.26	68.10	68.30	68.60	68.80	68.90
Wind Speed (m/s)	3.39	3.02	0.00	1.30	2.60	4.70	9.20

218
219

Table 2 Comparisons of WSIs concentrations with other high altitude and urban sites (mean, $\mu g/m^3$)

Sampling site	Sampling Year	SO_4^{2-}	NO_3^-	Na^+	NH_4^+	K^+	Ca^{2+}	Mg^{2+}	Reference
The QTP site									
Menyuan, Qinghan, the northeastern QTP (3295m)	2013	10.0	1.6	0.9	2.09	0.05	0.09	0.06	This study
South edge of the QTP (4276m)	2009	0.43	0.20	0.07	0.03	0.02	0.88	0.04	Cong et al. (2015)
Qilian Shan Station, the northeastern QTP (4180m)	2010	0.74	0.20	0.04	0.15	0.04	0.18	0.04	Xu et al. (2014)
Qinghai Lake, the northeastern QTP (3200m)	2010	4.45	0.38	0.13	-	0.12	0.23	0.06	Zhang et al. (2014)
	2012	3.65	1.42	0.26	0.62	0.10	0.66	0.10	Zhao et al. (2015)
Low altitude site in China (urban and background sites)									
Sampling site	Sampling Year	SO_4^{2-}	NO_3^-	Na^+	NH_4^+	K^+	Ca^{2+}	Mg^{2+}	Reference
Beijing (43m)	2013	13.80	15.43	0.69	8.02	1.06	0.08	0.58	Dao et al. (2014)
Shanghai (4m)	2009	12.9	15.0	-	6.64	0.94	-	-	Ming et al. (2017)
Xi'an (396m)	2006	42.0	20.6	-	13.1	-	-	-	Zhang et al. (2011)
Shangdianzi, Beijing (293m)	2009	8.68	11.20	-	3.23	-	-	-	Zhao et al. (2013a)
Lin'an, Zhejiang (138m)	2014	15.9	11.7	2.6	4.9	1.1	3.7	0.2	Zhang et al. (2017)
Other high-altitude area sites around the world									
Sampling site	Sampling Year	SO_4^{2-}	NO_3^-	Na^+	NH_4^+	K^+	Ca^{2+}	Mg^{2+}	Reference
Langtang, remote Himalayas, Nepal (3920m)	1999-2000	0.27	0.04	0.06	0.15	0.02	0.03	0.004	(Carrico et al., 2003)
Nagarkot, Kathmandu Valley, Nepal (2150m)	1999-2000	2.5	0.8	0.13	1.2	0.28	0.05	0.01	(Carrico et al., 2003)
Monte Martano, Italy (1100 m)	2009	1.90	0.84	0.02	0.54	0.06	0.25	0.06	(Moroni et al., 2015)
Great Basin National Park, Nevada, USA (2060 m)	2009-2012	0.38	0.10	-	-	-	0.05	-	(VanCuren and Gustin, 2015)

To better understand the concentrations of WSIs, we compared our observations with other studies implemented in background sites or urban sites across China and high altitude areas around the world in Table 2. Our results are lower as compared to studies in Europe and the USA (VanCuren and Gustin, 2015; Moroni et al., 2015), and the high latitude Himalaya region (Carrico et al., 2003); however, observations are comparable with some urban area in Nepal (Carrico et al., 2003). Observed

concentrations of SO_4^{2-} are also lower as compared to low altitude sites in China, for example urban sites in Beijing, Shanghai and Xi'an, and background sites in Shangdianzi (Beijing) and Lin'an (Zhejiang). Concentrations of NO_3^- were five to thirteen times lower as compared to those in low altitude areas (both urban and background sites), indicating that the influence of vehicle emissions in studying area is weak. NH_4^+ levels were lower as compared to those in urban sites (three to six times lower), and also slightly lower as compared to background sites (less than three times lower).

SNA concentrations in this study were higher as compared to those at other sites in the QTP, including the southern edge (Cong et al., 2015), Qilian Shan Station (Xu et al., 2014), and Qinghai Lake in the northeastern QTP (Zhang et al., 2014; Zhao et al., 2015). Large differences in concentrations suggest that the monitoring site in this study appears to be more impacted by natural and human activities as compared to other sites in the QTP.
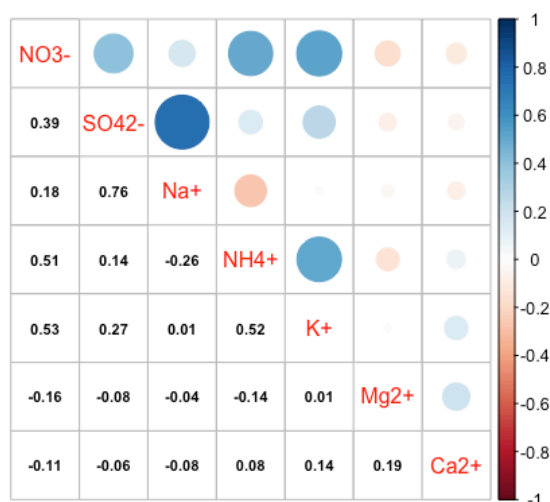
Figure 2 Correlation coefficients (r) between WSIs in $PM_{2.5}$ during sampling period

Correlations between WSIs are useful to investigate potential associations between the various WSIs (Xu et al., 2014). Figure 2 illustrates the correlation coefficients between WSIs based on their mass concentrations. A high correlation was found between Na^+ and SO_4^{2-} (r=0.76). Part of SO_4^{2-} and most of Na^+ could be attributed to the emission of the salt lake in our following discussion on source apportionment, which can explain the high correlation between SO_4^{2-} and Na^+. NO_3^- and SO_4^{2-} had a negative and weak correlation with Mg^{2+} and Ca^{2+}, which were found to be highly correlated with CO_3^{2-} in another study in the QTP (Xu et al., 2014). SNA displayed medium positive correlations with each other. K^+, commonly used as a marker for emissions from the burning of biomass or biofuel, had a medium correlation with NH_4^+ and NO_3^-.

To further examine the relationship between $PM_{2.5}$ and WSIs, we divided the $PM_{2.5}$ concentrations into four categories: a) $C(PM_{2.5}) < 20\mu g/m^3$, (b) $20\mu g/m^3 \leq C(PM_{2.5}) < 30\mu g/m^3$, (c) $30\mu g/m^3 \leq C(PM_{2.5}) < 40\mu g/m^3$, and (d) $C(PM_{2.5}) \geq 40\mu g/m^3$ and attributed each WSI measurement to its corresponding $PM_{2.5}$ category. Figure 3

shows the mean proportions of WSIs in PM$_{2.5}$ for the different categories. As the PM$_{2.5}$ concentration increases, the percentages of WSIs in PM$_{2.5}$ mass exhibited decreasing trends, suggesting that the contribution of WSIs to PM$_{2.5}$ increases was negligible. Therefore, more observational campaign should be implemented in the future to investigate the driver compositions on the increase of PM$_{2.5}$ mass concentrations.
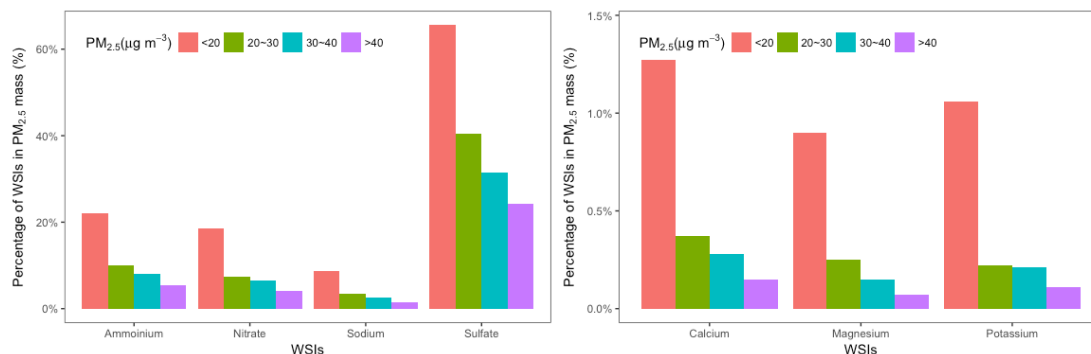
Figure 3 Mass portions of WSIs within different PM$_{2.5}$ level ranges

3.2 Source apportionment by PMF

In this study, all WSIs and gaseous pollutants were introduced into the PMF model for source identification. Five factors were used in the PMF model. The distributions of the factor species and the percentage of total species are shown in Figure 4.
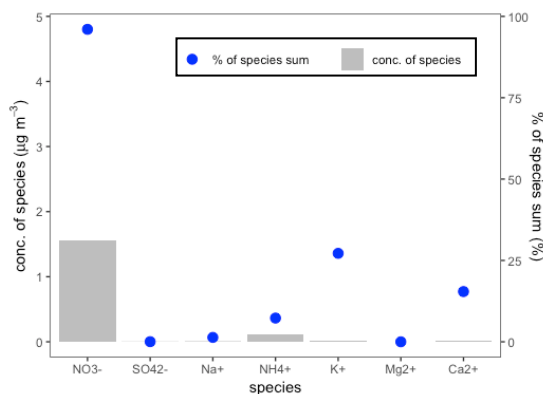

(a)

(b)

(c)
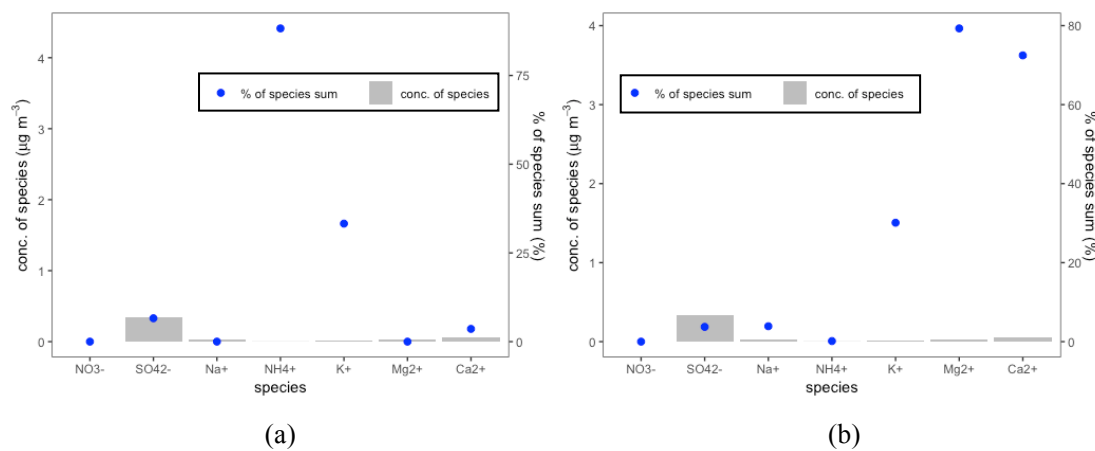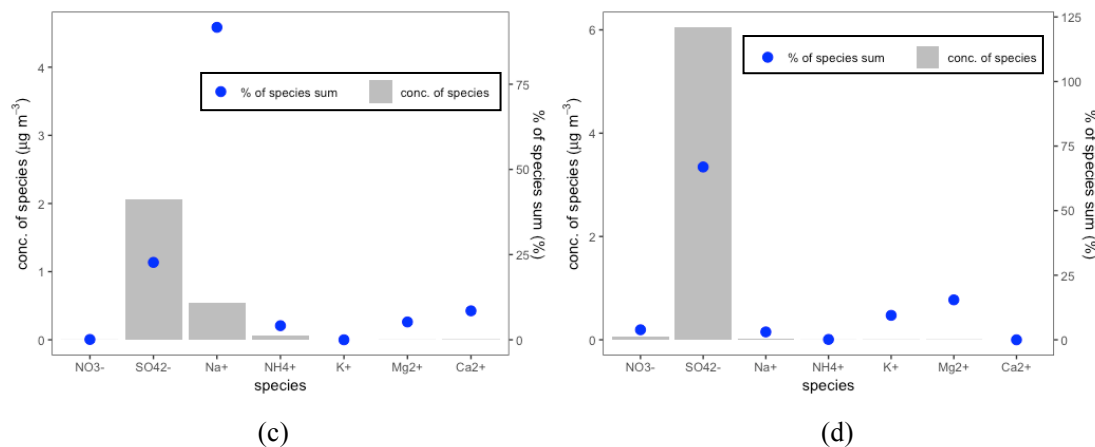
(d)

(e)

Figure 4 Source profiles exacted by PMF

(a) factor 1: animal waste emission and biomass burning; (b) factor 2: crustal dust; (c) factor 3: salt lake emissions; (d) factor 4: secondary sulfate and (e) factor 5: secondary nitrate (blue circle represents the percentage of species sum, while white bar represents concentration of species)

High NH_4^+ and K^+ loading were observed in factor 1. Livestock feces, which is commonly found in the meadows around the sampling site is a possible source of NH_4^+. K^+ can be attributed to the combustion of biomass, which has both natural and anthropogenic origins. Li et al. (2015) found that occasional biomass burning events in the area contributed significantly to the formation of anthropogenic fine particles.. Consequently, factor 1 is attributed to mixed sources, animal emissions and biomass burning, and crustal materials. Factor 2 is identified as crustal materials with high loading of Mg^{2+} and Ca^{2+} (Ma et al., 2003). Factor 3 has high Na^+ loading and a moderate SO_4^{2-} loading, which is also shown in previous correlation analysis with the correlation coefficient between SO_4^{2-} and Na^+ is 0.76. Our monitoring site is approximately 100 km from Qinghai Lake, a saline and alkaline water body which is the largest lake in China. Zhang et al. (2014) collected total suspended particle (TSP) and $PM_{2.5}$ samples at Qinghai Lake, and found that the concentration of Na^+ was higher as compared to other mountainous areas. Furthermore, they found that SO_4^{2-} was one the most abundant species in both TSP and $PM_{2.5}$. Therefore, we attribute factor 1 to aerosols emitted from Qinghai Lake. Factor 4 and 5 are enriched with SO_4^{2-} and NO_3^-, respectively, which could be considered as the secondary sulfate and secondary nitrate. The precursor of SO_4^{2-} is SO_2, which may originate from coal combustion, and NO_3^- is mainly converted from ambient NO_x, emitted by both vehicle exhaust and fossil fuel combustion.

3.2 Diurnal variation analysis

Diurnal variations of WSIs in $PM_{2.5}$, related gaseous pollutants (SO_2, NO_2, and O_3), and meteorological parameters (temperature, relative humidity, and wind speed) are shown in Figure 5.
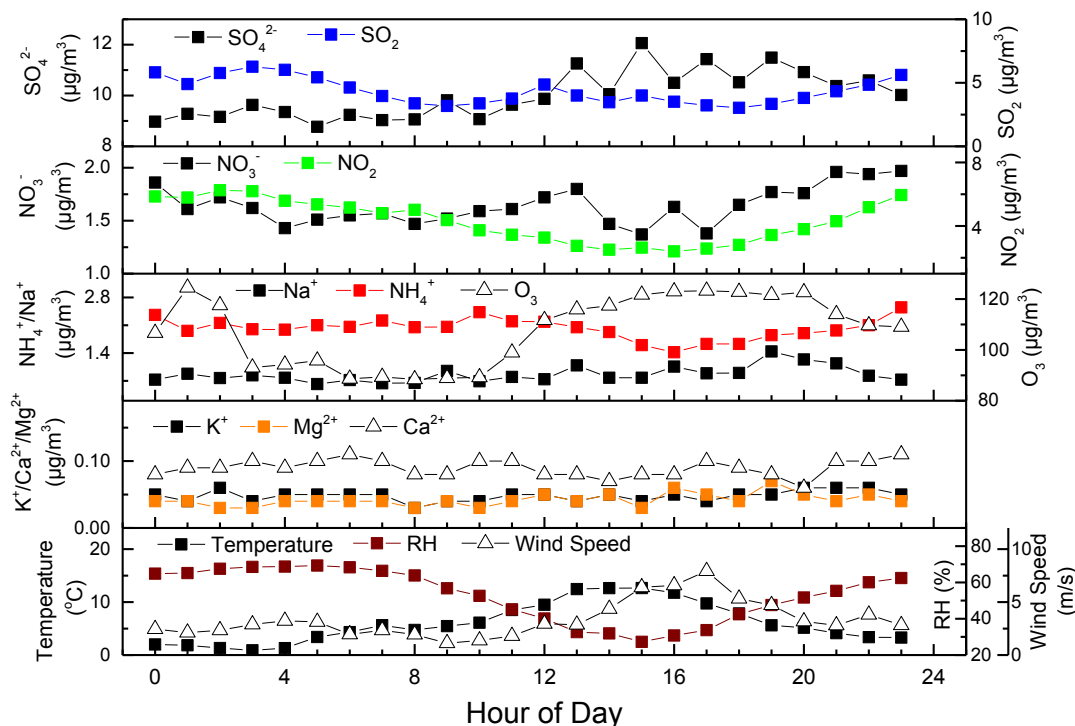
Figure5 Diurnal variations of WSIs in PM$_{2.5}$, gaseous pollutants (SO$_2$, NO$_2$, O$_3$), as well as meteorological parameters (temperature, relative humidity and wind speed) during sampling period

SO$_4^{2-}$ concentrations begin to increase from midnight (Beijing time), reach peak levels at approximately 15:00, and then decrease gradually. SO$_2$ concentrations exhibit a bimodal trend, with peaks at 03:00 and 12:00; conversely, SO$_4^{2-}$ exhibits an inverse trend. NO$_3^-$ concentrations peak at midnight and in the early afternoon, with lowest levels occurring during the late afternoon. NO$_2$ displays high nighttime levels and low daytime levels. NH$_4^+$ remains steady during the morning with a peak at 10:00, and then deceases until 16:00. O$_3$, temperature, RH, and wind speed also display evident diurnal variations; O$_3$, temperature, and wind speed are low (high) at night (day), while RH shows an inverse variation to this pattern.

3.3 Sulfate and nitrate oxidation ratio analysis

Average NOR and SOR during the whole measurement campaign were 0.16 and 0.55, respectively, suggesting potentially strong secondary formation of both SO$_4^{2-}$ and NO$_3^-$. Strong photochemical reactions and the existence of high O$_3$ concentrations would elevate the oxidant ratio from SO$_2$ and NO$_2$ to SO$_4^{2-}$ and NO$_3^-$, despite the low intensity of local emissions.

Variation trends of SOR and NOR were compared to changes in PM$_{2.5}$ concentration and ambient RH, as shown in Figure 6. Previous research has shown that, in urban areas, both SOR and NOR increased with the PM$_{2.5}$ concentration, suggesting that heavy PM$_{2.5}$ pollution corresponds to high SOR and NOR (Xu et al., 2017). However, studies investigating SOR and NOR variations at background sites with low PM$_{2.5}$ concentration range are rare. Our results showed that increasing concentrations of PM$_{2.5}$ at low levels corresponded to decreasing SOR and NOR

(Figure 6a), although the decreases were slight. This is consistent with our previous finding that concentrations of SO_4^{2-} and NO_3^- did not vary markedly with $PM_{2.5}$ increases at background sites, and provides further evidence to suggest that SO_4^{2-} and NO_3^- are not key drivers on the increase of $PM_{2.5}$ mass concentrations at low levels. Crustal materials are either not responsible for it as shown in Figure 3. The simultaneous observations of Du et al. (2015), indicated that organics were thought to be the major driver.

In Figure 6b, SOR initially decreases and then increases as RH increases. Peak SOR occurs when RH reaches both its maximum and minimum levels, when RH is low (10–20%), O_3 is high (114.6 μg/m^3, approximately the 70th percentile of O_3 concentrations), and vice versa (RH > 70% and O_3 93.8 μg/m^3, approximately the 30th percentile of O_3 concentrations). The formation of particulate SO_4^{2-} can be achieved via aqueous-phase oxidation (heterogeneous reaction) or gas-phase oxidation (photochemical reaction). Normally, aqueous-phase oxidation from SO_2 to SO_4^{2-} is faster than gas-phase oxidation (Wang et al., 2016). When RH is low and O_3 is high, the photochemical formation of SO_4^{2-} via gas-phase oxidation should be considered the main oxidation pathway. Conversely, low O_3 and high RH are not sufficient to provide adequate oxidizing capacity; thus photochemical SO_4^{2-} formation becomes less important and aqueous-phase oxidation plays a more dominant role.

NOR constantly decreases as RH increases. Particulate NO_3^- is predominantly formed by the gas-phase reaction of NO_2 and OH radicals during the day and by heterogeneous reactions of nitrate radicals (NO_3) at night (Seinfeld and Pandis, 2016). In this study, high (low) O_3 and low (high) RH lead to high (low) NOR, meaning that gas-phase reactions oxidized by high levels of O_3 are the major pathway for nitrate formation, while heterogeneous reactions play a less important role.
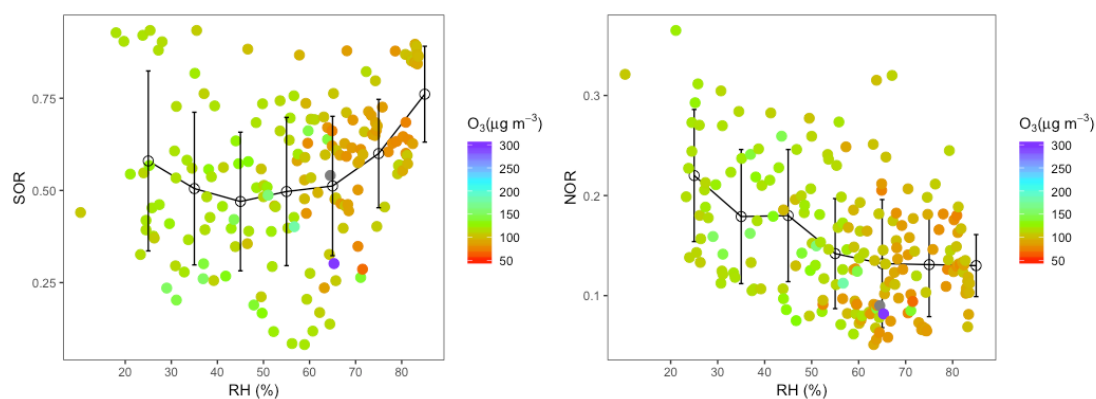

(a) PM$_{2.5}$

362

363   (b) RH
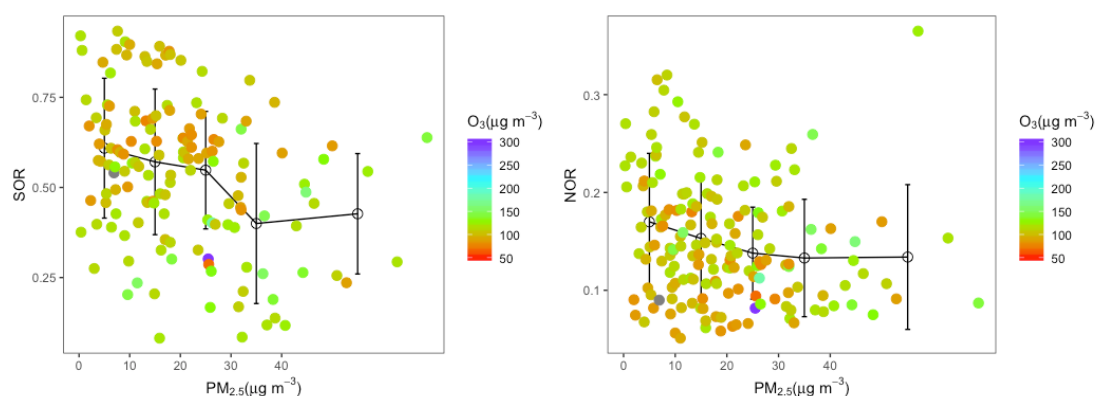
364   Figure 6 Variations of SOR and NOR as a function of $PM_{2.5}$ and RH. The vertical bars correspond

365   to one standard error from the mean.

366

367   Figure 7 characterizes the diurnal variations of SO_4^{2-}, NO_3^-, SOR, NOR, O_3, and

368   RH. The variation of SOR is small, particularly as compared to the evident diurnal

369   variation in SO_4^{2-}. Daytime gas-phase oxidation and nighttime aqueous-phase

370   oxidation are thought to be equally important to the formation of SO_4^{2-}. NOR is high

371   during the day and low at night; reflecting a strong positive correlation with O_3

372   (r=0.71, p<0.05) and a weak negative correlation with RH (r=-0.43, p<0.05). The high

373   correlation between NOR and O_3 indicates that gas-phase oxidation via

374   photochemical reactions is the main NO_3^- formation pathway. Trends of SOR and

375   NOR with RH and O_3 suggest that both photochemical and heterogeneous reactions

376   contribute to the secondary transformation of SO_2, while only photochemical reaction

377   drives the conversion of NO_2 to nitrate.

378   It is apparent that photochemical reactions (dominated by O_3 oxidization)

379   contribute markedly to the secondary conversion of both SO_2 and NO_2, while

380   heterogeneous reactions (promoted by the existence of aqueous phase) contributed to

381   the formation of SO_4^{2-} and only had a weak effect on NO_3^-. Ma et al. (2003) found

382   that fine nitrate particles (Dp < 2.0 μm) at Waliguan Observatory (150 km south of

383   our monitoring site) were most likely produced via gaseous-phase reactions between

384   nitric acid and ammonia, in line with our findings on nitrate formation.
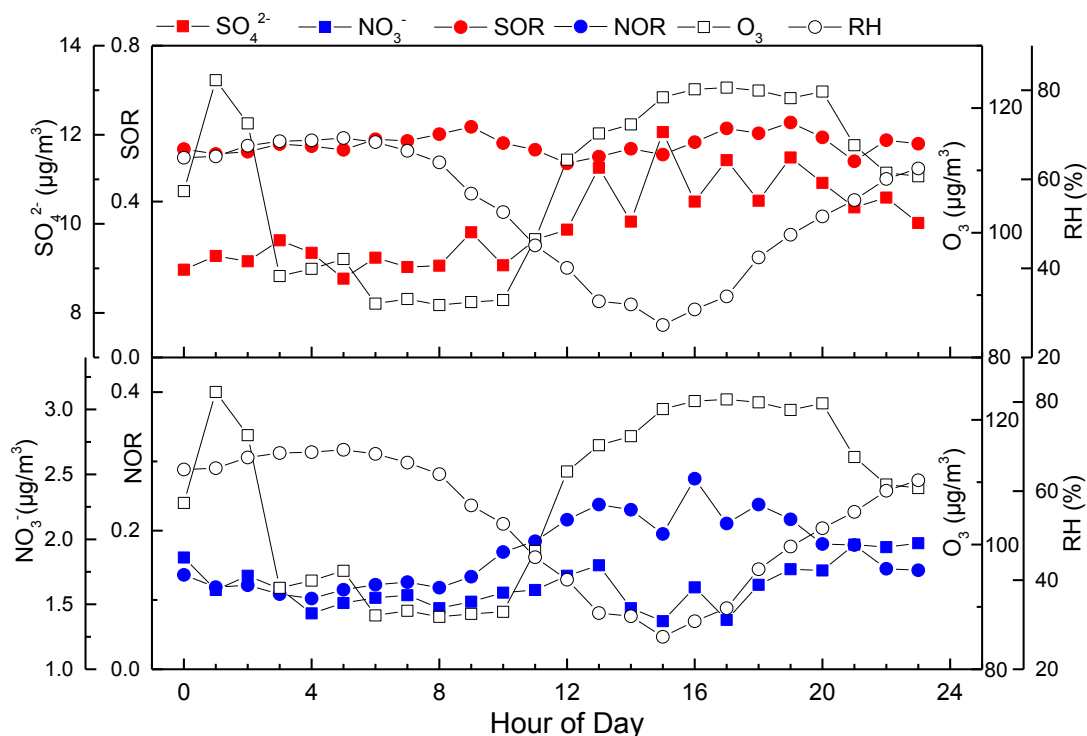
Figure 7 Diurnal variations of SO_4^{2-} and NO_3^-, SOR, NOR O_3 and RH during sampling period

3.4 Molecular composition of major ionic species

The molecular chemical forms of the major WSIs in $PM_{2.5}$ were identified using bivariate correlations based on individual WSI molar concentrations (Verma et al., 2010; Wang et al., 2005). In this study, we used equivalent concentrations for correlation analysis, and the coefficients are shown in Table 3. Figure 8 a–c show scatter plots of the equivalent concentrations of $[NH_4^+]$ and $[NO_3^-]$, $[Na^+]$ and $[SO_4^{2-}]$, and $[NH_4^+]$ and $[SO_4^{2-} + NO_3^-]$, respectively. $(NH_4)_2SO_4$ and NH_4NO_3 are major components of atmospheric aerosols (Park et al., 2004), commonly formed by the neutralization of sulfuric acid (H_2SO_4) and nitric acid (HNO_3) by NH_3 (Xu et al., 2014). It is apparent that NH_4^+ is closely correlated with NO_3^- (r=0.56). The slope of the regression between NH_4^+ and NO_3^- ($\mu ep/m^3$ versus $\mu ep/m^3$) is 2.28, indicating the complete neutralization of NO_3^- by NH_4^+. SO_4^{2-} was highly correlated with Na^+ (r=0.56), rather than NH_4^+. Unlike NO_3^- and NH_4^+, Na^+ was completely neutralized by SO_4^{2-} (slope=0.15) in the form of $NaHSO_4$. Excess NH_4^+ would then combine with excess SO_4^{2-} (r=0.46). The regression slope between excess NH_4^+ and excess SO_4^{2-} was 0.72, meaning that excess NH_4^+ was completely neutralized by SO_4^{2-} and existed in the form of $(NH_4)_2SO_4$. Excess sulfuric acid was likely neutralized by crustal WSIs; and K_2SO_4 was a major chemical species in aerosol particles based on their correlation coefficients. Good regression results between $[NH_4^+ + Na^+ + K^+]$ and $[NO_3^- + SO_4^{2-}]$ were also observed in Figure 8 d.
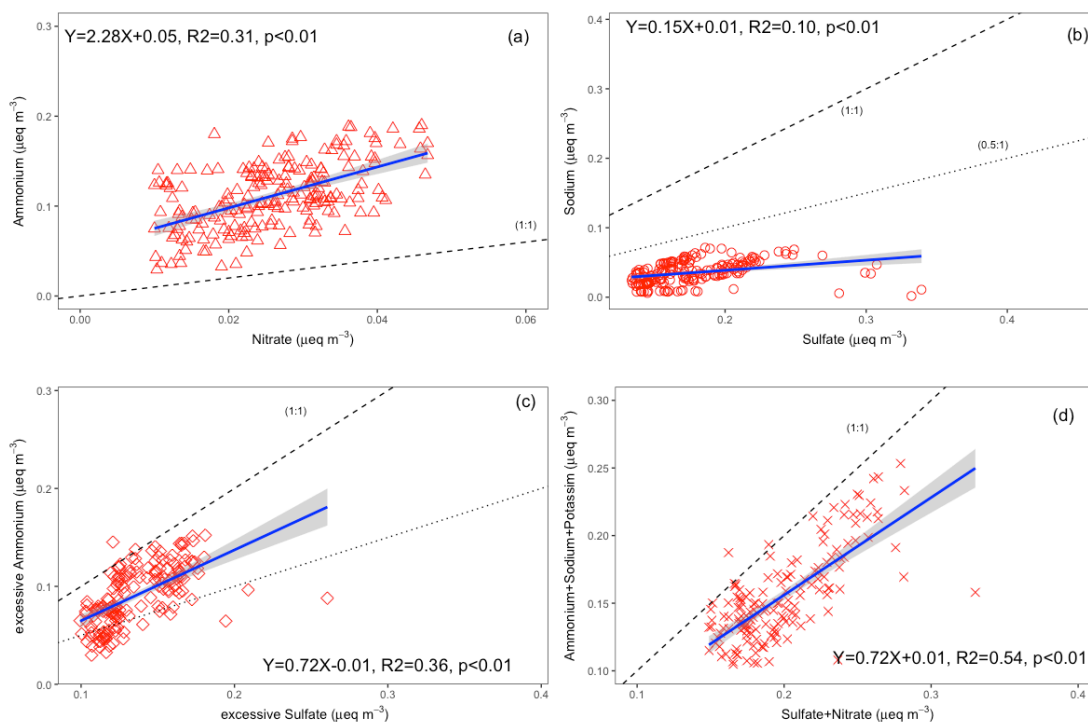
Table 3 Correlation coefficients (r) between the equivalent concentrations of WSIs in $PM_{2.5}$ during sampling period

	NO_3^-	SO_4^{2-}	Na^+	NH_4^+	K^+	Mg^{2+}	Ca^{2+}

	NO_3^-	SO_4^{2-}	Na^+	NH_4^+	K^+	Mg^{2+}
NO_3^-						
SO_4^{2-}	0.49					
Na^+	0.17	0.56				
NH_4^+	0.56	0.46	-0.24			
K^+	0.56	0.39	0.06	0.57		
Mg^{2+}	-0.11	-0.13	-0.06	-0.15	-0.03	
Ca^{2+}	-0.06	-0.11	0.01	-0.08	0.03	0.09

410

411

412

Figure 8 Scatter plot of (a) $[NH_4^+]$ and $[NO_3^-]$ (b) $[Na^+]$ and $[SO_4^{2-}]$ (c) [excessive NH_4^+] and [excessive SO_4^{2-}] (d) $[NH_4^+ + Na^+ + K^+]$ and $[NO_3^- + SO_4^{2-}]$

3.5 Ion acidity analysis

The ion balance, expressed by the sum of the equivalent concentration ($\mu eq/m^3$) ratio of cation to anion (C/A), is an indicator of the acidity of particulate matter (Wang et al., 2005). In this study, the ion balance ratio was 0.87, indicating that aerosols tended to be acid, in line with previous studies in the QTP (Xu et al., 2015; Zhao et al., 2015). However, the results across the QTP are quite different at different locations. In the studies of south edge of the QTP, the aerosols were found to be alkaline at Qomolangma (Mt. Everest) Station for Atmospheric and Environmental Observation and Research Station (TSP, C/A=4.1) (Cong et al., 2015), four sites in central Himalayan region (TSP, C/A=3.7) (Tripathee et al., 2017), and Shigatsz, China (PM2.1, C/A=1.5) (Yang et al., 2016). While in the studies of the northeastern QTP, the results vary. Two studies at Qilan Shan Station (QSS) at different time achieved difference values of C/A (C/A=1.3, sampling time: summer, 2011; C/A=0.95, sampling time: summer, 2012) (Xu et al., 2014; Xu et al., 2015). Another study at the Qinghai Lake also got slightly acidic result ($PM_{2.5}$, C/A=0.8) (Zhao et al.,

431 2015). In their study at the summer of 2012, Xu et al. (2015) also found that the
432 equivalent balances of water-soluble species in different size modes indicate that the
433 accumulation mode particles were somewhat acidic (with the linear regression slope
434 of [$NH4^+$+Ca^{2+}+Mg^{2+}+K^+] vs. [SO_4^{2-}+NO_3^-] being 0.6) and that the coarse mode
435 particles were almost neutral (the slope was 0.999), indicating that small size of
436 particles show tendency of acid. As compared to the results at the south edge of the
437 QTP that is mostly influenced by natural emission (such as mineral dust), the
438 northeastern QTP suffers more anthropogenic emissions (e.g. SO_4^{2-} and NO_3^-), since it
439 is more close to the areas with intensive human activities.

440 Figure 9 shows the scatter and linear regression plot of cations and anions
441 ($\mu eq/m^3$). It is apparent that most points are below the 1:1 line, highlighting the acid
442 tendency. The total equivalent anion concentration was regressed against the total
443 equivalent concentrations of cations, and the slope of regression was 0.58.
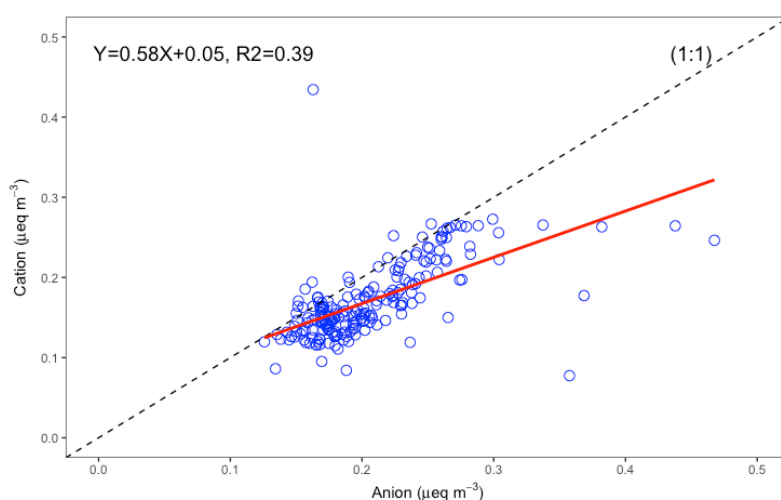
444

445 Figure 9 Cation and Anion scatter plot and linear regression

446

447 Aerosol acidity for different categories of $PM_{2.5}$ concentration (described in
448 section 3.1) and their respective scatter plots of total equivalent concentrations of
449 anions and cations are shown in Figure 10. C/A was high when $PM_{2.5}$ concentrations
450 exceeded $20\mu g/m^3$, indicating that aerosol acidity was weak when the $PM_{2.5}$
451 concentration was high. This provides further evidence to support our finding that
452 SO_4^{2-} and NO_3^- did not contribute to $PM_{2.5}$ increases.
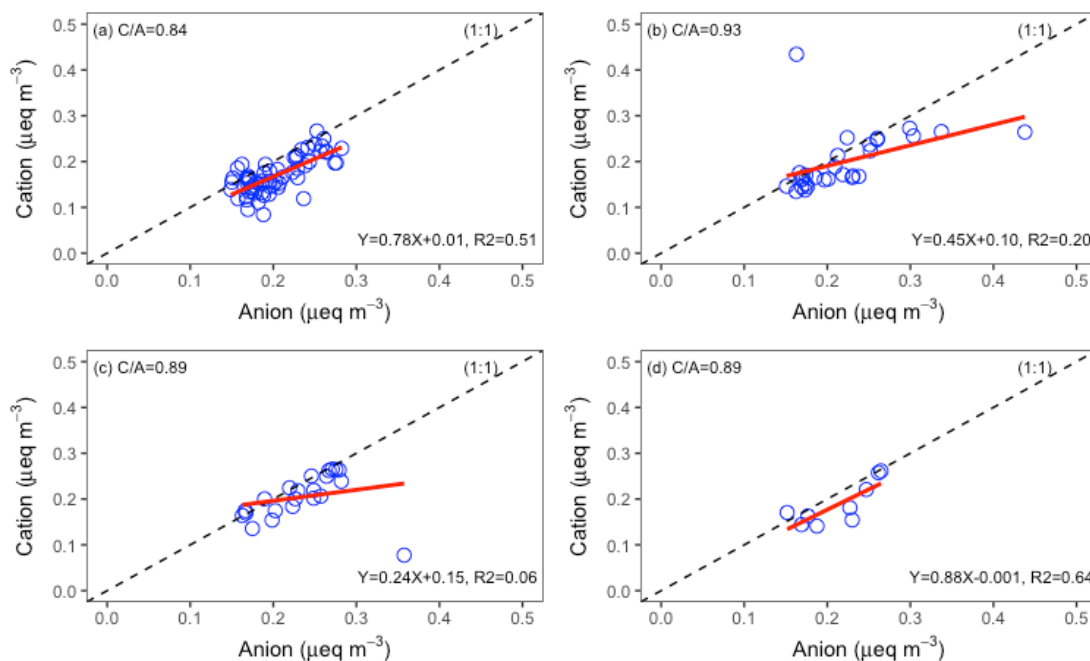
Figure 10 Scatter plot Σ Anion and Σ Cation with different $PM_{2.5}$ concentration range (a) $C(PM_{2.5})$ < 20μg/m³ (b) 20μg/m³ ≤ $C(PM_{2.5})$ <30μg/m³ (c) 30μg/m³ ≤ $C(PM_{2.5})$ <40μg/m³ (d) $C(PM_{2.5})$ ≥ 40μg/m³

4. Conclusion

The QTP is an ideal location for characterizing aerosol properties. In this study, we investigated the characterizations of WSIs associated with autumn $PM_{2.5}$ at a background site (3295 m a.s.l.) in the QTP. In this study, we finished some analysis on WSIs by taking advantage of real-time data to: 1) analyze the diurnal variations of WSIs; 2) discuss the formation of secondary sulfate and nitrate at the QTP; and 3) investigate source apportionment on hourly data within short-term observation. All these above are difficult by using traditional manual PM2.5 sampling, given that it usually takes hours or even days for sample collection, and is unable to detect more variations on aerosol compositions and supply more data on finer temporal scale for further analysis.

During our observation, we collected real time concentrations of WSIs, and analyzed them together with $PM_{2.5}$, gaseous pollutants, and meteorological parameters for investigating ion chemistry of aerosols in the QTP. SO_4^{2-}, NO_3^-, and NH_4^+ (SNA) were the three most abundant WSI species, and crust-originated ions (Na^+, Mg^{2+}, K^+, and Ca^{2+}) comprised a small fraction of total WSIs. As compared to similar studies in China, SNA concentrations in this study were lower as compared to low altitude urban areas, but higher relative to other sites in the QTP. NH_4NO_3, $(NH_4)_2SO_4$, Na_2SO_4, and K_2SO_4 are found to be the major atmospheric aerosol components during our observation campaign.

Source apportionment using a PMF model identified five factors: mixed factor including animal waste emission and biomass burning, crustal dust, salt lake emissions, secondary sulfate and secondary nitrate. Based on the results of source

apportionment, we found that the major sources of sulfate are salt lake emission and secondary transformation, while particulate nitrate is mostly from secondary conversion. After excluding the emission of sulfate from the salt lake, we investigated the possible formation pathway of SO_4^{2-} and NO_3^-, the concentrations of which showed evident diurnal variations. The results revealed that strong solar intensity and high O_3 concentrations combined with low daytime RH greatly enhanced the conversion of SO_2 and NO_2 to SO_4^{2-} and NO_3^-, respectively. Heterogeneous reactions were weak overnight, and contributed to SO_4^{2-} formation only. Our analysis suggests that photochemical reactions played a critical role in the secondary formation of SO_4^{2-} and NO_3^- during our observation period.

To our knowledge, there is no such real-time measurement on WSIs associated with $PM_{2.5}$ at rural sites in the QTP yet. This study provides some preliminary results on aerosol ion compositions on the QTP, and proposes the potential formation mechanism of secondary sulfate and nitrate. These findings are supposed to be useful for further studies on aerosol chemistry in this area.

Data Availability

All data of this work can be obtained from Bin Han (hanbin@craes.org.cn)

Author Contributions

BH, WY and ZB designed the experiments. BY, XW and XD were in charge of the whole field experiment. JW and XZ processed the original data and primary analysis. BH prepared the manuscript with contributions from all co-authors.

Reference

Cao, J. J., Lee, S. C., Chow, J. C., Watson, J. G., Ho, K. F., Zhang, R. J., Jin, Z. D., Shen, Z. X., Chen, G. C., Kang, Y. M., Zou, S. C., Zhang, L. Z., Qi, S. H., Dai, M. H., Cheng, Y., and Hu, K.: Spatial and seasonal distributions of carbonaceous aerosols over China, J. Geophys. Res.-Atmos., 112, 10.1029/2006jd008205, 2007.

Carrico, C. M., Bergin, M. H., Shrestha, A. B., Dibb, J. E., Gomes, L., and Harris, J. M.: The importance of carbon and mineral dust to seasonal aerosol properties in the Nepal Himalaya, Atmos. Environ., 37, 2811-2824, https://doi.org/10.1016/S1352-2310(03)00197-3, 2003.

Cong, Z., Kang, S., Kawamura, K., Liu, B., Wan, X., Wang, Z., Gao, S., and Fu, P.: Carbonaceous aerosols on the south edge of the Tibetan Plateau: concentrations, seasonality and sources, Atmos. Chem. Phys., 15, 1573-1584, 10.5194/acp-15-1573-2015, 2015.

Dao, X., Wang, Z., Lv, Y., Teng, E., Zhang, L., and Wang, C.: Chemical Characteristics of Water-Soluble Ions in Particulate Matter in Three Metropolitan Areas in the North China Plain, PLOS ONE, 9, e113831, 10.1371/journal.pone.0113831, 2014.

Du, W., Sun, Y. L., Xu, Y. S., Jiang, Q., Wang, Q. Q., Yang, W., Wang, F., Bai, Z.

P., Zhao, X. D., and Yang, Y. C.: Chemical characterization of submicron aerosol and particle growth events at a national background site (3295 m a.s.l.) on the Tibetan Plateau, Atmos. Chem. Phys., 15, 10811-10824, 10.5194/acp-15-10811-2015, 2015.

Frege, C., Bianchi, F., Molteni, U., Trostl, J., Junninen, H., Henne, S., Sipila, M., Herrmann, E., Rossi, M. J., Kulmala, M., Hoyle, C. R., Baltensperger, U., and Dommen, J.: Chemical characterization of atmospheric ions at the high altitude research station Jungfraujoch (Switzerland), Atmos. Chem. Phys., 17, 2613-2629, 10.5194/acp-17-2613-2017, 2017.

Gao, Y., and Anderson, J. R.: Characteristics of Chinese aerosols determined by individual-particle analysis, J. Geophys. Res.-Atmos., 106, 18037-18045, 10.1029/2000jd900725, 2001.

Gong, Z. H., Lan, Z. J., Xue, L., Zeng, L. W., He, L. Y., and Huang, X. F.: Characterization of submicron aerosols in the urban outflow of the central Pearl River Delta region of China, Frontiers of Environmental Science & Engineering, 6, 725-733, 10.1007/s11783-012-0441-8, 2012.

He, L. Y., Huang, X. F., Xue, L., Hu, M., Lin, Y., Zheng, J., Zhang, R. Y., and Zhang, Y. H.: Submicron aerosol analysis and organic source apportionment in an urban atmosphere in Pearl River Delta of China using high-resolution aerosol mass spectrometry, J. Geophys. Res.-Atmos., 116, 10.1029/2010jd014566, 2011.

Jiang, Q., Sun, Y. L., Wang, Z., and Yin, Y.: Aerosol composition and sources during the Chinese Spring Festival: fireworks, secondary aerosol, and holiday effects, Atmos. Chem. Phys., 15, 6023-6034, 10.5194/acp-15-6023-2015, 2015.

Jin, L. Y., Ganopolski, A., Chen, F. H., Claussen, M., and Wang, H. J.: Impacts of snow and glaciers over Tibetan Plateau on Holocene climate change: Sensitivity experiments with a coupled model of intermediate complexity, Geophysical Research Letters, 32, 10.1029/2005gl023202, 2005.

Kopacz, M., Mauzerall, D. L., Wang, J., Leibensperger, E. M., Henze, D. K., and Singh, K.: Origin and radiative forcing of black carbon transported to the Himalayas and Tibetan Plateau, Atmos. Chem. Phys., 11, 2837-2852, 10.5194/acp-11-2837-2011, 2011.

Li, J. J., Wang, G. H., Wang, X. M., Cao, J. J., Sun, T., Cheng, C. L., Meng, J. J., Hu, T. F., and Liu, S. X.: Abundance, composition and source of atmospheric PM2.5 at a remote site in the Tibetan Plateau, China, Tellus Series B-Chemical and Physical Meteorology, 65, 10.3402/tellusb.v65i0.20281, 2013.

Li, W. J., Chen, S. R., Xu, Y. S., Guo, X. C., Sun, Y. L., Yang, X. Y., Wang, Z. F., Zhao, X. D., Chen, J. M., and Wang, W. X.: Mixing state and sources of submicron regional background aerosols in the northern Qinghai–Tibet Plateau and the influence of biomass burning, Atmos. Chem. Phys., 15, 13365-13376, 10.5194/acp-15-13365-2015, 2015.

Ma, J. Z., Tang, J., Li, S. M., and Jacobson, M. Z.: Size distributions of ionic aerosols measured at Waliguan Observatory: Implication for nitrate gas-to-particle transfer processes in the free troposphere, J. Geophys. Res.-Atmos., 108, 10.1029/2002jd003356, 2003.

McGregor, G. R.: Climate variability and change in the Sanjiangyuan region, in:

Landscape and ecosystem diversity, dynamics and management in the Yellow River Source Zone, Springer, 35-57, 2016.

Ming, L., Jin, L., Li, J., Fu, P., Yang, W., Liu, D., Zhang, G., Wang, Z., and Li, X.: PM2.5 in the Yangtze River Delta, China: Chemical compositions, seasonal variations, and regional pollution events, Environ. Pollut., 223, 200-212, https://doi.org/10.1016/j.envpol.2017.01.013, 2017.

Moroni, B., Castellini, S., Crocchianti, S., Piazzalunga, A., Fermo, P., Scardazza, F., and Cappelletti, D.: Ground-based measurements of long-range transported aerosol at the rural regional background site of Monte Martano (Central Italy), Atmospheric Research, 155, 26-36, 10.1016/j.atmosres.2014.11.021, 2015.

Paatero, P., and Tapper, U.: Positive matrix factorization: A non-negative factor model with optimal utilization of error estimates of data values, Environmetrics, 5, 111-126, 10.1002/env.3170050203, 1994.

Paatero, P.: Least squares formulation of robust non-negative factor analysis, Chemometrics and Intelligent Laboratory Systems, 37, 23-35, http://dx.doi.org/10.1016/S0169-7439(96)00044-5, 1997.

Park, R. J., Jacob, D. J., Field, B. D., Yantosca, R. M., and Chin, M.: Natural and transboundary pollution influences on sulfate-nitrate-ammonium aerosols in the United States: Implications for policy, J. Geophys. Res.-Atmos., 109, 10.1029/2003jd004473, 2004.

Schulte, P., and Arnold, F.: PYRIDINIUM IONS AND PYRIDINE IN THE FREE TROPOSPHERE, Geophysical Research Letters, 17, 1077-1080, 10.1029/GL017i008p01077, 1990.

Seinfeld, J. H., and Pandis, S. N.: Atmospheric chemistry and physics: from air pollution to climate change, John Wiley & Sons, 2016.

Shen, R. Q., Ding, X., He, Q. F., Cong, Z. Y., Yu, Q. Q., and Wang, X. M.: Seasonal variation of secondary organic aerosol tracers in Central Tibetan Plateau, Atmos. Chem. Phys., 15, 8781-8793, 10.5194/acp-15-8781-2015, 2015.

Su, F. G., Duan, X. L., Chen, D. L., Hao, Z. C., and Cuo, L.: Evaluation of the Global Climate Models in the CMIP5 over the Tibetan Plateau, Journal of Climate, 26, 3187-3208, 10.1175/jcli-d-12-00321.1, 2013.

Sun, Y. L., Wang, Z. F., Fu, P. Q., Yang, T., Jiang, Q., Dong, H. B., Li, J., and Jia, J. J.: Aerosol composition, sources and processes during wintertime in Beijing, China, Atmos. Chem. Phys., 13, 4577-4592, 10.5194/acp-13-4577-2013, 2013.

Sun, Y. L., Wang, Z. F., Du, W., Zhang, Q., Wang, Q. Q., Fu, P. Q., Pan, X. L., Li, J., Jayne, J., and Worsnop, D. R.: Long-term real-time measurements of aerosol particle composition in Beijing, China: seasonal variations, meteorological effects, and source analysis, Atmos. Chem. Phys., 15, 10149-10165, 10.5194/acp-15-10149-2015, 2015.

Tang, J., Wen, Y., Zhou, L., Qi, D., Zheng, M., Trivett, N., and Erika, W.: Observational study of black carbon in clean air area of western China (in Chinese), Q. J. Appl. Meteorol., 10, 160-170, 1999.

Tripathee, L., Kang, S. C., Rupakheti, D., Zhang, Q. G., Huang, J., and Sillanpaa, M.: Water-Soluble Ionic Composition of Aerosols at Urban Location in the Foothills

of Himalaya, Pokhara Valley, Nepal, Atmosphere, 7, 10.3390/atmos7080102, 2016.

Tripathee, L., Kang, S. C., Rupakheti, D., Cong, Z. Y., Zhang, Q. G., and Huang, J.: Chemical characteristics of soluble aerosols over the central Himalayas: insights into spatiotemporal variations and sources, Environ. Sci. Pollut. Res., 24, 24454-24472, 10.1007/s11356-017-0077-0, 2017.

VanCuren, R., and Gustin, M. S.: Identification of sources contributing to PM2.5 and ozone at elevated sites in the western US by receptor analysis: Lassen Volcanic National Park, California, and Great Basin National Park, Nevada, Science of the Total Environment, 530, 505-518, 10.1016/j.scitotenv.2015.03.091, 2015.

Vedantham, R., Landis, M. S., Olson, D., and Pancras, J. P.: Source Identification of PM2.5 in Steubenville, Ohio Using a Hybrid Method for Highly Time-Resolved Data, Environmental Science & Technology, 48, 1718-1726, 10.1021/es402704n, 2014.

Verma, S. K., Deb, M. K., Suzuki, Y., and Tsai, Y. I.: Ion chemistry and source identification of coarse and fine aerosols in an urban area of eastern central India, Atmospheric Research, 95, 65-76, 10.1016/j.atmosres.2009.08.008, 2010.

Wan, X., Kang, S., Wang, Y., Xin, J., Liu, B., Guo, Y., Wen, T., Zhang, G., and Cong, Z.: Size distribution of carbonaceous aerosols at a high-altitude site on the central Tibetan Plateau (Nam Co Station, 4730ma.s.l.), Atmospheric Research, 153, 155-164, http://dx.doi.org/10.1016/j.atmosres.2014.08.008, 2015.

Wang, G. H., Zhang, R. Y., Gomez, M. E., Yang, L. X., Zamora, M. L., Hu, M., Lin, Y., Peng, J. F., Guo, S., Meng, J. J., Li, J. J., Cheng, C. L., Hu, T. F., Ren, Y. Q., Wang, Y. S., Gao, J., Cao, J. J., An, Z. S., Zhou, W. J., Li, G. H., Wang, J. Y., Tian, P. F., Marrero-Ortiz, W., Secrest, J., Du, Z. F., Zheng, J., Shang, D. J., Zeng, L. M., Shao, M., Wang, W. G., Huang, Y., Wang, Y., Zhu, Y. J., Li, Y. X., Hu, J. X., Pan, B., Cai, L., Cheng, Y. T., Ji, Y. M., Zhang, F., Rosenfeld, D., Liss, P. S., Duce, R. A., Kolb, C. E., and Molina, M. J.: Persistent sulfate formation from London Fog to Chinese haze, Proceedings of the National Academy of Sciences of the United States of America, 113, 13630-13635, 10.1073/pnas.1616540113, 2016.

Wang, Y., Zhuang, G. S., Tang, A. H., Yuan, H., Sun, Y. L., Chen, S. A., and Zheng, A. H.: The ion chemistry and the source of PM2.5 aerosol in Beijing, Atmos. Environ., 39, 3771-3784, 10.1016/j.atmosenv.2005.03.013, 2005.

Wen, Y., Xu, X., Tang, J., Zhang, X., and Zhao, Y.: Enrichment Characteristics and Origin of Atmospheric Aerosol Elements at Mt Waliguan (in Chinese), Q. J. Appl. Meteorol., 12, 400-408, 2001.

Wu, Z. J., Hu, M., Liu, S., Wehner, B., Bauer, S., Ssling, A. M., Wiedensohler, A., Petaja, T., Dal Maso, M., and Kulmala, M.: New particle formation in Beijing, China: Statistical analysis of a 1-year data set, J. Geophys. Res.-Atmos., 112, 10.1029/2006jd007406, 2007.

Xu, J., Wang, Z., Yu, G., Qin, X., Ren, J., and Qin, D.: Characteristics of water soluble ionic species in fine particles from a high altitude site on the northern boundary of Tibetan Plateau: Mixture of mineral dust and anthropogenic aerosol, Atmospheric Research, 143, 43-56, http://dx.doi.org/10.1016/j.atmosres.2014.01.018, 2014.

Xu, J. Z., Zhang, Q., Wang, Z. B., Yu, G. M., Ge, X. L., and Qin, X.: Chemical composition and size distribution of summertime PM$_{2.5}$ at a high altitude remote location in the northeast of the Qinghai–Xizang (Tibet) Plateau: insights into aerosol sources and processing in free troposphere, Atmos. Chem. Phys., 15, 5069-5081, 10.5194/acp-15-5069-2015, 2015.

Xu, L., Duan, F., He, K., Ma, Y., Zhu, L., Zheng, Y., Huang, T., Kimoto, T., Ma, T., Li, H., Ye, S., Yang, S., Sun, Z., and Xu, B.: Characteristics of the secondary water-soluble ions in a typical autumn haze in Beijing, Environ. Pollut., 227, 296-305, 10.1016/j.envpol.2017.04.076, 2017.

Yang, K., Wu, H., Qin, J., Lin, C. G., Tang, W. J., and Chen, Y. Y.: Recent climate changes over the Tibetan Plateau and their impacts on energy and water cycle: A review, Global and Planetary Change, 112, 79-91, 10.1016/j.gloplacha.2013.12.001, 2014.

Yang, Y. J., Zhou, R., Yan, Y., Yu, Y., Liu, J. Q., Di, Y. A., Du, Z. Y., and Wu, D.: Seasonal variations and size distributions of water-soluble ions of atmospheric particulate matter at Shigatse, Tibetan Plateau, Chemosphere, 145, 560-567, 10.1016/j.chemosphere.2015.11.065, 2016.

Yao, T., Thompson, L. G., Mosbrugger, V., Zhang, F., Ma, Y., Luo, T., Xu, B., Yang, X., Joswiak, D. R., Wang, W., Joswiak, M. E., Devkota, L. P., Tayal, S., Jilani, R., and Fayziev, R.: Third Pole Environment (TPE), Environmental Development, 3, 52-64, http://dx.doi.org/10.1016/j.envdev.2012.04.002, 2012.

Zhang, N., Cao, J., Liu, S., Zhao, Z., Xu, H., and Xiao, S.: Chemical composition and sources of PM2.5 and TSP collected at Qinghai Lake during summertime, Atmospheric Research, 138, 213-222, 10.1016/j.atmosres.2013.11.016, 2014.

Zhang, N. N., Cao, J. J., Ho, K. F., and He, Y. Q.: Chemical characterization of aerosol collected at Mt. Yulong in wintertime on the southeastern Tibetan Plateau, Atmospheric Research, 107, 76-85, 10.1016/j.atmosres.2011.12.012, 2012.

Zhang, T., Cao, J. J., Tie, X. X., Shen, Z. X., Liu, S. X., Ding, H., Han, Y. M., Wang, G. H., Ho, K. F., Qiang, J., and Li, W. T.: Water-soluble ions in atmospheric aerosols measured in Xi'an, China: Seasonal variations and sources, Atmospheric Research, 102, 110-119, https://doi.org/10.1016/j.atmosres.2011.06.014, 2011.

Zhang, Y., Zhang, H., Deng, J., Du, W., Hong, Y., Xu, L., Qiu, Y., Hong, Z., Wu, X., Ma, Q., Yao, J., and Chen, J.: Source regions and transport pathways of PM2.5 at a regional background site in East China, Atmos. Environ., 167, 202-211, https://doi.org/10.1016/j.atmosenv.2017.08.031, 2017.

Zhao, P. S., Dong, F., He, D., Zhao, X. J., Zhang, X. L., Zhang, W. Z., Yao, Q., and Liu, H. Y.: Characteristics of concentrations and chemical compositions for PM2.5 in the region of Beijing, Tianjin, and Hebei, China, Atmos. Chem. Phys., 13, 4631-4644, 10.5194/acp-13-4631-2013, 2013a.

Zhao, Z. Z., Cao, J. J., Shen, Z. X., Xu, B. Q., Zhu, C. S., Chen, L. W. A., Su, X. L., Liu, S. X., Han, Y. M., Wang, G. H., and Ho, K. F.: Aerosol particles at a high-altitude site on the Southeast Tibetan Plateau, China: Implications for pollution transport from South Asia, J. Geophys. Res.-Atmos., 118, 11360-11375, 10.1002/jgrd.50599, 2013b.

697   Zhao, Z. Z., Cao, J. J., Shen, Z. X., Huang, R. J., Hu, T. F., Wang, P., Zhang, T.,
698   and Liu, S. X.: Chemical composition of PM2.5 at a high-altitude regional
699   background site over Northeast of Tibet Plateau, Atmos. Pollut. Res., 6, 815-823,
700   10.5094/apr.2015.090, 2015.

701   Zhou, Y., Wang, T., Gao, X. M., Xue, L. K., Wang, X. F., Wang, Z., Gao, J. A.,
702   Zhang, Q. Z., and Wang, W. X.: Continuous observations of water-soluble ions in
703   PM2.5 at Mount Tai (1534 ma.s.l.) in central-eastern China, Journal of Atmospheric
704   Chemistry, 64, 107-127, 10.1007/s10874-010-9172-z, 2009.

705
706